The Unique Molecular Behavior of Water at the Chloroform–Water Interface

CATHRYN L. McFEARIN and GERALDINE L. RICHMOND*

Department of Chemistry, University of Oregon, 1253 University of Oregon, Eugene, Oregon 97403

The molecular bonding and orientation of water at the chloroform–water interface has been examined in this study using vibrational sum-frequency spectroscopy (VSFS). The results provide a key puzzle piece towards our understanding of the systematic changes in the interfacial bonding and orientation of water that occur with variations in the polarity of the organic phase, especially when compared with previous studies of different liquid–liquid interfacial systems. In these VSFS studies the OH spectral responses of interfacial water molecules are used to characterize the interactions between water and the organic phase. The spectral analysis, aided by isotopic dilution studies, shows that the moderate polarity of the chloroform phase results in a mixed interfacial region with stronger organic–water bonding and fewer bonding interactions between adjacent water molecules than was previously found for studies of nonpolar organic liquid–water interfaces. Even with the more mixed interfacial region and stronger organic–water interactions, interfacial water retains a significant amount of orientational ordering. These results are compared with recent predictions from molecular dynamics simulations about how molecules behave at the chloroform–water interface.

Index Headings: **Liquid–liquid interfaces; Water; Hydrophobic surfaces; Hydrogen bonding; Vibrational sum-frequency spectroscopy; VSFS.**

INTRODUCTION

The chloroform–water interface is widely used in extraction processes because the slightly polar nature of the chloroform allows more selective separation of molecules than is possible with other organic–liquid systems. In industrial applications chloroform is used in the extraction and purification of antibiotics, alkaloids, and vitamins.[1] In biology the chloroform–water interface forms the basis for isolating DNA, RNA, and proteins.[2] The properties that make the chloroform–water interface effective and important in extraction also make it important for understanding the fundamental interactions present between two largely immiscible liquids and how these interactions affect the interfacial properties, including transport of molecules and ions across the interface. An increasing number of theoretical[3–12] and experimental[13–22] studies have emerged in recent years that seek to understand the properties and structuring of water near a hydrophobic surface on a molecular level. However, very few theoretical and even fewer experimental studies have explored how the behavior of water and the interfacial properties change as the polarity of the hydrophobic phase is progressively increased, which is important in achieving a more comprehensive understanding of organic–water interfacial properties.

These studies report the experimental investigation of the molecular structure and bonding of water at the chloroform–water interface using vibrational sum-frequency spectroscopy (VSFS). Although there have been studies investigating chloroform adsorbed on ice or in vacuum,[23–25] a detailed experimental study of the condensed fluid phase chloroform–water interface has yet to be carried out to our knowledge. By examining the OH stretch modes of the interfacial water molecules, different types of hydrogen-bonded water species can be discerned and characterized with regards to their interfacial structuring. Previous studies have shown the value of VSFS in exploring how water bonds and structures near a hydrophobic organic liquid and the weak interactions that exist between interfacial water and organic molecules.[26–32] The chloroform–water interfacial system, with the relatively small dipole moment of chloroform (1.04 D), provides an interesting intermediate case, from a polarity perspective, compared to other systems studied thus far, including water next to nonpolar (CCl_4 and *n*-alkanes)[26,30,31] liquids, the more polar liquid 1,2-dichloroethane (DCE) with a dipole moment of 2.1 D in the gauche form,[32] and mixtures of CCl_4 with chloroform, DCE, and dichloromethane (DCM), which has a dipole moment of 1.6 D.[28] The results of the chloroform–water interface presented here are derived from detailed analysis absent from some of the previous experimental studies[28,32] of liquid–liquid interfaces. They provide a key element in our understanding of the progression of molecular interactions that occur at these liquid–liquid interfaces upon variation of the polarity of the organic phase that has not been learned from these previous studies.

The results of these experimental studies also provide an interesting comparison with theoretical investigations that have arisen from several recent computational efforts. Of particular relevance are calculations of the chloroform–water interface that use molecular dynamics (MD) simulations to calculate VSF spectra and allow direct comparisons between experimental and computational spectra.[33] These MD simulations build on the knowledge base and experience of MD simulations by Benjamin[3,4,11] as well as Chang and Dang,[7–10] and VSF spectral calculations for water by Morita and Hynes.[34] Population densities and orientations of different types of water-bonded species at the interface are calculated in good agreement with previously published MD results[3,4,7–11,35,36] and are then used in the calculation of a VSF spectrum for comparison with experiment.[33,37] Information complementary to the experimental results can be extracted from the MD simulations including the types of water-bonded species that contribute to different regions of the VSF spectrum, the interfacial depths of these species, and their orientations. Other MD studies by Hore et al. have focused on elucidating the intertwined interfacial behaviors of both the water *and* the organic molecules (not accessible in past VSFS studies) for several hydrophobic–aqueous interfaces through calculation of the order parameters of these molecules as a function of the distance from the interface.[38–40] Jedlovszky and co-workers investigated the structure of some of these liquid–liquid

Received 2 March 2010; accepted 3 June 2010.
* Author to whom correspondence should be sent. E-mail: richmond@uoregon.edu.

0003-7028/10/6409-0986$2.00/0

interfaces by utilizing Monte Carlo simulation methods in a similar manner to the studies by Hore et al.[35,36] The chloroform–water interface has been used by Wipff and coworkers as a model oil–aqueous interface for studying liquid–liquid extraction phenomena and partitioning of ions via numerous simulation studies.[41–45]

Vibrational sum-frequency spectroscopy has been shown to be a powerful technique for studying buried interfaces, and liquid–liquid interfaces are no exception.[29] In the current VSFS study, isotopic mixtures of H_2O and D_2O are employed in the aqueous phase to assist in understanding the general types of bonding between interfacial molecules in the VSF spectrum. Isotopic dilution aids in identification of the types of water species that contribute to the VSF spectrum and narrows down their peak frequencies. Although there is still H_2O present in the aqueous phase, the interfacial spectrum of the OH region is simplified, with interfacial HOD molecules making more of a contribution.[31,46,47] This assists in more accurate spectral fitting and also allows for comparison with other liquid–liquid systems that have been studied in a similar manner.

VIBRATIONAL SUM-FREQUENCY SPECTROSCOPY BACKGROUND

Because VSFS is described extensively in the literature, only an outline of the important aspects is given here.[48–54] In VSFS two beams are overlapped at an interface, generating a third beam at the sum of the frequencies of the two incident beams. For the experiments presented here, one beam is at a fixed visible frequency and one is tunable over a range of infrared (IR) frequencies. The intensity $I(\omega_{SF})$ of the VSFS light generated at the interface is given by

$$I(\omega_{SF}) \propto |\chi^{(2)}_{eff}|^2 I(\omega_{IR}) I(\omega_{VIS}) \quad (1)$$

where $I(\omega_{IR})$ and $I(\omega_{VIS})$ are the respective intensities of the incoming tunable infrared and visible beams and $\chi^{(2)}_{eff}$ is the effective macroscopic second order nonlinear susceptibility. The susceptibility term $\chi^{(2)}$ is related to the effective term via the Fresnel factors and unit polarization vectors. $\chi^{(2)}$ is composed of a non-resonant term, $\chi^{(2)}_{NR}$, and a resonant susceptibility term, $\chi^{(2)}_{\upsilon}$:

$$\chi^{(2)} \propto \chi^{(2)}_{NR} + \sum_{\upsilon} \chi^{(2)}_{\upsilon} \quad (2)$$

A non-resonant contribution has not been detected in these liquid–liquid studies. The resonant portion can be written as

$$\chi^{(2)}_{\upsilon} \propto \frac{NA_{\upsilon}}{\omega_{\upsilon} - \omega_{IR} - i\Gamma_{\upsilon}} \quad (3)$$

where N is the number density of molecules, A_{υ} is the product of the Raman and IR transition moments, ω_{υ} is the vibrational transition frequency, ω_{IR} is the tunable IR frequency, and Γ_{υ} is the linewidth of the transition. As the IR is tuned over a range of frequencies and ω_{IR} approaches a resonance ω_{υ}, there is an increase in VSFS intensity, producing a vibrational spectrum. Generally these susceptibility terms are complex quantities that have both phases and amplitudes, which give rise to VSFS intensity that, as shown in Eqs. 1 and 2, is the square of the sum of the terms. The resulting spectrum can have either constructive or destructive interferences between contributions from different interfacial modes.

The macroscopic term $\chi^{(2)}_{\upsilon}$ is related to the microscopic property, the molecular hyperpolarizability β, by Eq. 4 via the number density of the molecules probed, N, and their orientation:

$$\chi^{(2)}_{\upsilon} = \frac{N}{\varepsilon_0} \langle \beta \rangle \quad (4)$$

The angular brackets denote an ensemble average over different molecular orientations.

As shown in the equations above, the VSFS signal intensity is dependent on several factors including interfacial molecular orientation, number density, and the strengths of the transition modes. The intensity also depends on the polarizations chosen for the input visible, IR, and generated sum-frequency beams. By choosing different polarization combinations, different elements of the tensor are probed. All spectra shown in this work were taken in the *ssp* polarization combination, which probes the $\chi^{(2)}_{yyz}$ element. The polarization notation denotes the sum-frequency, visible, and IR beams, respectively. The *ssp* combination of input and output beams probes those vibrational modes that have a component of their transition dipole perpendicular to the interfacial plane.

EXPERIMENTAL DETAILS AND ANALYSIS

The laser system used for these experiments comprises a 532 nm visible beam generated by frequency doubling the fundamental output from a Nd:YAG laser (30 ps pulse width, 10 Hz, manufactured by EKSPLA). The IR beam was generated from an optical parametric generation/amplification and difference frequency system (EKSPLA) based on BBO and $AgGaS_2$ crystals that is tunable from 1000 to 4300 cm^{-1}.

The sample cell has been described previously.[31] It consists of a hollow cylinder made from Kel-F and mounted on an IR grade fused silica prism. The visible and IR beams were overlapped at the liquid–liquid interface at angles of 23.7° and 19° from the horizontal plane, respectively. These angles align the beams in a total internal reflection (TIR) geometry, which is used to maximize the VSFS signal.[55] Pulse energies used for the visible and IR beams are 80 μJ and ~140 μJ, respectively. A series of optics composed of two edge filters (Semrock) and one notch filter (Kaiser Optical Systems), a lens, polarizer, and waveplate (all from EKSPLA) filter out reflected 532-nm light, focus the sum-frequency beam, and select the desired sum-frequency polarization, respectively. The VSFS signal is then sent through a monochromator and detected by a photomultiplier tube.

The spectra of the liquid–liquid interface are especially susceptible to the effects of contaminants. Therefore, these experiments used high purity liquids: CCl_4 (Aldrich, ≥99.9% CHROMASOLV HPLC grade) and chloroform-d (Aldrich 99.8% d atom). Deuterated chloroform was chosen in place of $CHCl_3$ because it does not have the CH absorption in the spectral region used for the experiments. Because the $CDCl_3$ can break down upon prolonged light exposure, bottles were wrapped in foil and refrigerated while not in use. The liquid was allowed to come to room temperature in the dark before use in the VSFS measurements. The H_2O used for the aqueous phase came from a Barnstead Nanopure II system (18 MΩ cm). The D_2O used in the isotopic dilution measurements was purchased from Cambridge Isotope Laboratories (99.9% d atom). All measurements presented here were taken at room

temperature. The sample cell and all glassware used in the experiments were soaked in concentrated sulfuric acid containing NoChromix and then rinsed thoroughly with the Nanopure filtered water before use.

The following steps were taken during and after VSF spectral acquisition to ensure that the most accurate data possible was obtained. First, because the VSFS intensity is dependent on the incoming beam energies, they were measured before each spectrum was taken and adjusted as needed to keep the energies constant. Second, multiple spectra were taken of each interface and averaged together on a given day to obtain a greater signal-to-noise ratio for the spectra. Spectra were also taken over several days in order to assure reproducibility and average out any slight changes in beam overlap or focusing that might affect the spectral intensity. Third, the spectra were normalized to account for both variations in IR energy resulting from the generation processes and the small absorption of IR energy at $\sim$3600 cm^{-1} by the fused silica prism. The spectra were normalized by taking spectra of the nonresonant sum-frequency response of an uncoated gold mirror in place of the aqueous phase but still in contact with the respective organic liquid (either CCl_4 or chloroform) and dividing them into the spectra taken in step two. Fourth, the Fresnel factors and unit vectors were calculated for the different interfaces' spectra taken in the *ssp* polarization scheme.[56] Values for the real refractive indices of the fused silica in both the visible and IR were used in the Fresnel factor calculations.[57] In addition, the calculations assumed real and constant indices of refraction for both the CCl_4 and chloroform liquids (1.4607 and 1.4419, respectively) based on their transparency through the spectral regions used in the current experiments.[58,59] The real and imaginary values of the indices of refraction for water in both the visible and IR energy regions were used.[60] Previous analysis of isotopic dilution spectra at the air–water interface have shown that the use of Fresnel factors incorporating D_2O and HOD indices of refraction did not significantly change the conclusions, so they were not used here.[61] The beam angles used in the calculations were those cited above. The normalized spectra from step three were then divided by these corrections. After all these steps, the resulting spectra are $|\chi^{(2)}|^2$, not $|\chi^{(2)}_{\text{eff}}|^2$, which allows for a more direct comparison between VSF spectra.

Finally, the spectra were fit to an expression for $|\chi^{(2)}|^2$ that accounts for the homogeneous broadening (Lorentzian line shape) and inhomogeneous broadening (Gaussian line shape) that results from the complex molecular environment found at the liquid–liquid interface.[62,63] As mentioned in the previous section, the VSFS intensity is related to the coherent square of the sum of the resonant susceptibility terms. Therefore, the resulting spectrum can have either constructive or destructive interferences between contributions from different interfacial modes. Fitting the spectrum is necessary in order to account for these interferences because they can distort the shape and apparent frequency of the spectral peaks. The fit assigns a Lorentzian and a Gaussian width, a center frequency, an amplitude, and a phase to each peak.

With so many parameters and several peaks present, uncertainty arises in the credibility of the resulting parameters. To reduce this uncertainty, isotopic dilution experiments were carried out to aid in the deconvolution of the OH interfacial spectrum. This method has been used for both the air–water[46,47] and CCl_4–water[31] interfaces. Using mixtures of H_2O and D_2O removes intermolecular coupling between the two OH oscillators by forming HOD, thereby greatly simplifying the complex spectrum of the OH region. Additionally, by varying the ratio of HOD, H_2O, and D_2O there are several spectra that can be iteratively fit using a global fitting analysis that constrains many of the above parameters for each spectrum, thereby giving a more rigorous analytical fit to the data.[46] Equilibrium mole fraction (mf) concentrations of H_2O, D_2O, and HOD were calculated using the volumes of liquid delivered, the bulk densities of H_2O and D_2O, and assuming an equilibrium constant of 4.[46] It should be noted that results from spectral fitting of the air–water interface differ from those of work utilizing phase-sensitive VSFS techniques.[47] Specifically, the lower frequency region of the spectrum shows different phase results for the two methods. However, this technique has not been extended to examination of the liquid–liquid interface. Characterization of the broad spectral responses from water is still under debate, both in the interfacial community and for bulk water. The current study of the chloroform–water interface focuses primarily on the portion of the VSF spectrum (higher frequencies) where there is the least degree water bonding occurring because it comes from those water molecules directly in contact with the other liquid phase and therefore is our probe of the interfacial interactions taking place.

Results from previously published MD simulated VSF spectra both from our laboratory[37,64] and others[65] are in agreement with the assignments made for these liquid–liquid and air–water interfaces for the spectra with the highest concentration of HOD and D_2O. However, with increased H_2O concentration the simulations demonstrate that more complicated bonding comes into play, making distinct spectral assignments impossible due to broad overlapping bands from all water-bonded species. For this reason we view the peaks derived from the fits for pure H_2O as representing collections of weak and strong bonding modes rather than assigning specific, single modes to a particular peak.

RESULTS AND DISCUSSION

The VSF spectrum of water in the OH stretch region for the chloroform–water interface is shown in Fig. 1a. As noted above, the interface possesses structural and mixing qualities that are intermediate between those of the CCl_4–water and DCE– (or DCM–) water interfaces that have been previously studied and characterized by VSFS.[28,30–32] Thus the CCl_4–water and DCE–water spectra are shown in Figs. 1b and 1c, respectively, for comparison. Although the DCE–water spectrum was obtained using a different VSFS laser system[32] and the Fresnel factors were not removed, the spectrum was scaled accordingly so that a direct comparison with the chloroform and CCl_4 interfaces could be made. These experimental details do not affect the appearance of the spectrum but are merely noted here. The spectra share some similar features corresponding to different water OH vibrational modes originating from the variety of water species that are present at the interface. Our current understanding of the general features in the spectrum has been derived from previous studies of other liquid–liquid systems that have been a combination of both experimental[26–29,31,32] and computational VSFS[33,37,64,66,67] studies. The DCE–water interface (Fig. 1c) does not show distinct spectral features due to the nature of the polar organic liquid–water interactions occurring at the

interface, as explained later in the paper. As such, the comparisons drawn below will be primarily between the chloroform–water and CCl_4–water spectra (Figs. 1a and 1b).

For the spectra in Figs. 1a and 1b a sharp, intense peak exists at the high-frequency end of the spectrum denoted as region **1** in the figure. Both spectra also show significant intensity between 3300–3600 cm^{-1} (labeled region **2**). The sharp peak in these spectra is attributed to those water molecules in the interfacial region that have a single OH oscillator oriented into the organic phase. The peak in region **1** is referred to here as the free OH mode. It acts as an uncoupled oscillator because its companion OH bond is oriented into the aqueous phase where it can hydrogen bond to other water molecules, thereby reducing its oscillator energy and broadening the spectral width. This companion OH bond has been designated in previous VSFS liquid–liquid studies as the "donor OH" mode because it has the capacity and orientation to act as a proton donor to surrounding water molecules. Isotopic dilution studies of the CCl_4–water interface indicate that the donor OH mode makes a significant contribution to the intensity in region **2**.[31] Computational VSF spectra for both the CCl_4– and chloroform–water interfaces suggest that for non-deuterated water systems, the most significant contribution to region **2** is indeed donor water molecules that are doubly bound to other water molecules, as both a proton donor through the H and an electron donor through the O.[33] We label water molecules participating in these two bonds as "OH" bonded species.[37] For simplicity in the discussion to follow we will refer to region **2** as the donor OH peak. The simulations also show that there are other contributing species of smaller populations in spectral region **2**,[37] most of which also possess a weaker hydrogen bonding character. The spectral responses from these less coordinated modes (including those that "straddle" the interface and contain a free OH) make up the majority of VSFS intensity in regions **1** and **2** for the chloroform–water and CCl_4–water spectra shown. The intensity of the weakly bound species in these spectra comes from the highly oriented nature of the straddling water molecules that have the majority of their transition dipole moment in the plane normal to the interface, which is selectively probed by the choice of beam polarizations used here (*ssp*).

The spectra in Figs. 1a and 1b also show a smaller spectral contribution at lower frequencies (labeled **3** in Fig. 1). For liquid–liquid interfaces studied thus far, region **3** represents contributions from water molecules in the interfacial region that have more coordinated hydrogen bonding geometries.[26,28,31,32] Calculated VSF spectra show that the water species contributing to this region are dominated by those with stronger bonding characteristics, such as those that act as double hydrogen bond donors in addition to being electron pair donors,[33] and originate from water molecules found a bit deeper into the interfacial region.[67] Spectral region **3** is also likely to contain contributions from collective motions as has been suggested for air–water systems.[68,69] For simplicity, region **3** of the spectrum will be referred to as the higher coordinated water region consisting of a mixture of molecules with a greater number of and/or stronger hydrogen bonding interactions.

Although the spectra shown in Figs. 1a and 1b share similarities, the more interesting information lies in the differences. From inspection there appears to be a ~25 cm^{-1} red-shift in the free OH peak for the chloroform–water spectrum compared to the CCl_4–water spectrum, indicative of stronger water–chloroform interactions at the interface. Another obvious difference is in the relative intensities of regions **1** and **2** for the two different interfaces. For the CCl_4–water interfacial spectrum, region **1** is more intense than region **2**. A sharp dip in intensity near 3600 cm^{-1} is present in the chloroform–water spectrum that is not apparent in the CCl_4–water interfacial spectrum. Because of the coherent nature of the VSFS response and accompanying complex spectral interferences, understanding the source of this dip as well as the frequencies of the free and donor OH modes requires

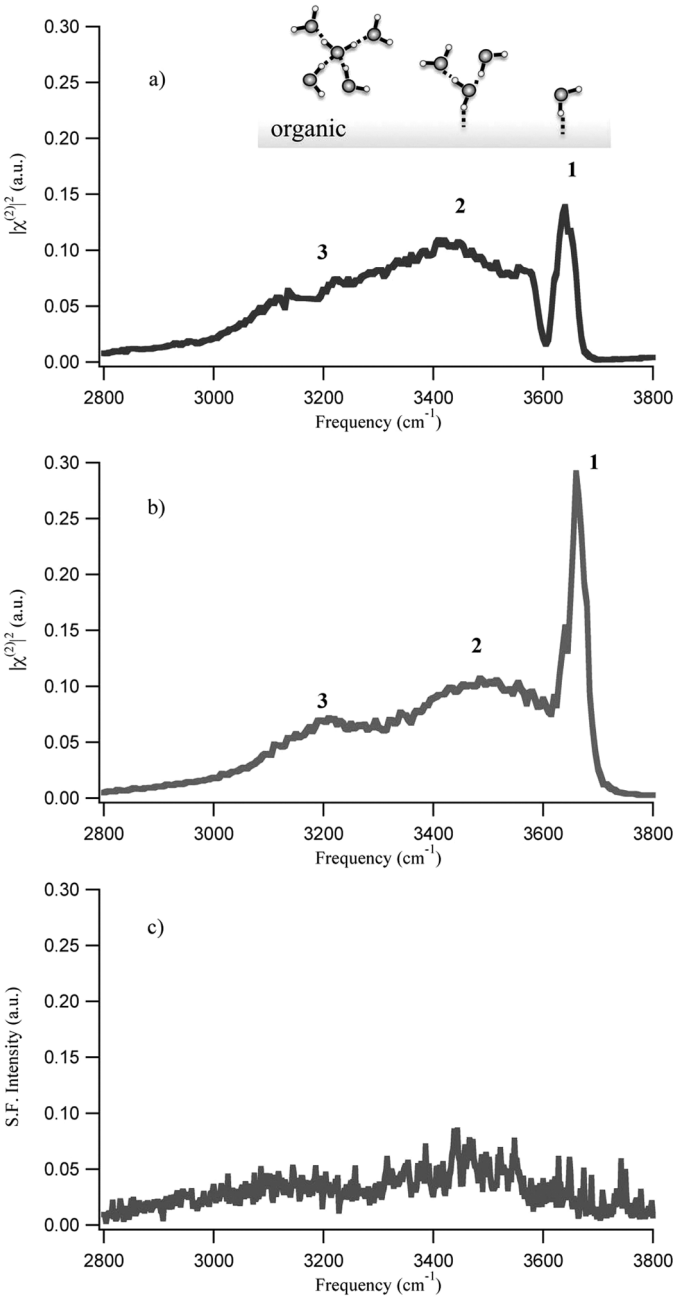

FIG. 1. VSF spectra of the (**a**) chloroform–water, (**b**) CCl_4–water, and (**c**) DCE–water interfaces taken in the *ssp* polarization scheme. The different OH spectral regions are represented numerically. (**1**) Free OH mode, red-shifted ~25 cm^{-1} for (b) compared to (a). (**2**) Donor OH mode, and (**3**) higher coordinated modes. The schematic depicts each region pictorially by showing interfacial water molecule bonding represented by dashed lines.

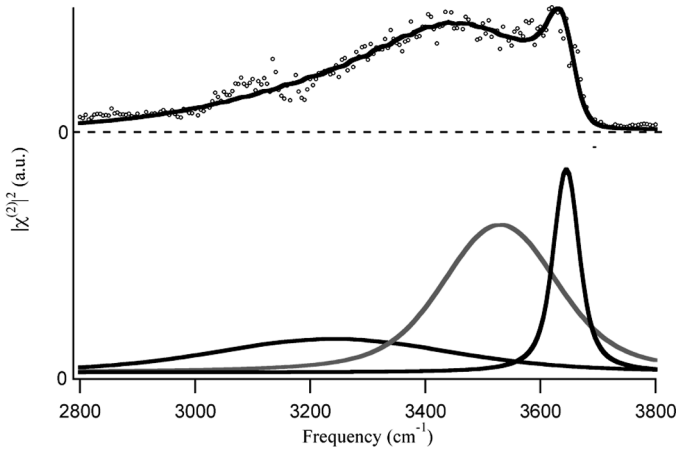

FIG. 2. Fitting results for the VSF spectrum of the 0.46 mf HOD + 0.42 mf D_2O–chloroform interface. The top plot shows the data (circles) with the fit (solid line). The bottom plot shows the individual peak contributions: free OH, donor OH, and higher coordinated modes from highest to lowest energies, respectively.

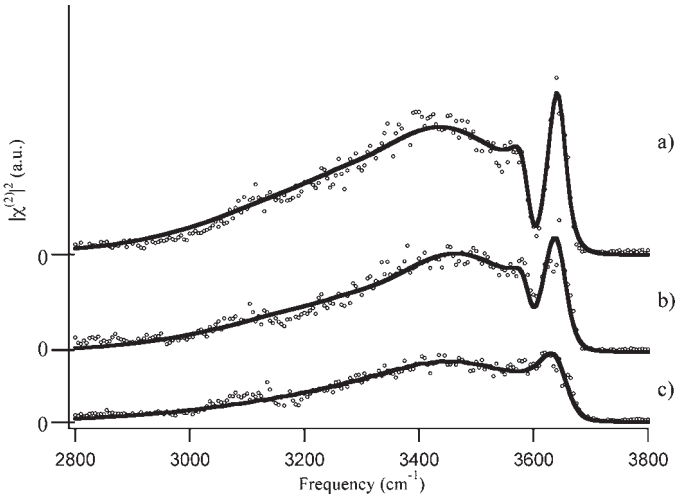

FIG. 3. VSF spectra of the interface of chloroform with (***a***) H_2O, (***b***) 0.20 mf D_2O + 0.49 mf HOD, and (***c***) 0.42 mf D_2O + 0.46 mf HOD. Circles are the data points and the solid line denotes the best fit to the data.

further spectral analysis. These effects are taken into account by spectral fitting, beginning with the isotopic dilution spectra. Spectral assignments are more accurate under conditions of minimal intra- and intermolecular coupling, such as with isotopic dilution, which is employed here along with global spectral fitting routines.

Figure 2 contains the data collected for chloroform at the interface with a mixture of 0.46 mf HOD, and 0.42 mf D_2O. This system can be fit most accurately because much of the intramolecular coupling is removed by the difference in atomic masses of the hydrogen and deuterium of HOD, making it the simplest spectrum to fit. Spectra acquired at higher concentrations of D_2O gave too little intensity to be fit accurately. The spectrum of the chloroform–D_2O interface showed zero intensity, indicating a zero non-resonant contribution to the VSFS response. For the isotopic mixture containing 0.46 mf HOD, more of the spectral intensity should come from the OH of HOD molecules either interacting with chloroform or other water molecules. The spectrum can then be fit primarily to two peaks, a free and donor OH, with a very small contribution from the more highly coordinated water region. The spectrum and resulting fit line are shown in the top portion of Fig. 2. In order to be consistent with other analyses, the Lorentzian widths[46] and phase relationships[70] of the peaks were held to values determined in previous VSFS experiments. The peaks that comprise the fit are shown in the bottom portion of Fig. 2. These results determine the peak frequencies that are used in fitting the other H_2O–D_2O mixture spectrum and the chloroform–H_2O spectrum.

Figures 3a through 3c show the spectra of the chloroform–H_2O, chloroform–0.49 mf HOD, and chloroform–0.46 mf HOD interfaces with their respective fits. They are offset vertically for clarity. As the concentration of H_2O increases, going from Figs. 3c to 3a, the intensities of the free and donor OH peaks increase, as does the intensity in region **3**. Increases in peak amplitudes from a greater number of OH oscillators and also in significant broadening (increase in the Gaussian widths) of the peaks known to occur because of the increased number of various H_2O–H_2O interactions that take place with increased H_2O concentration[46,64] contribute to the increased intensity. Additionally, a sharp dip begins to appear in Fig. 3b at ~3600 cm^{-1} that was not seen in the highest HOD concentration spectrum, Fig. 3c. The additional sharp contribution must necessarily arise from (1) water molecules that have weak interactions on the order of what is observed for the nearby free OH, and (2) from water molecules with intramolecularly coupled OH bonds since they were not apparent at the highest HOD concentrations. Initial attempts at fitting the spectra in Figs. 3a and 3b used only the three peaks discussed above for Fig. 3a. However, changes to the peak parameters, both physically reasonable and not, resulted in fits that did not reproduce the sharp dip at ~3600 cm^{-1}. The only way to account for this spectral feature was to add a fourth peak to the fitting routine. This new peak will be discussed in more detail later in this section.

The spectrum of the chloroform–water interface with the fit line and its composite peaks based on the isotopic dilution experiments are shown in Figs. 4a and 4b, respectively. The broad peak found at the lowest frequency (region **3**) is from those water molecules with the greatest hydrogen bonding character and is centered at 3240 cm^{-1}. This frequency is very close to the value determined for the same peak at the CCl_4–water interface in a previous, similar analysis.[31] Additionally the intensity in this spectral region for both the chloroform–water and CCl_4–water interfacial spectra are very similar (region **3** in Figs. 1a and b). This indicates that those water molecules that are participating in a more highly coordinated hydrogen bonding geometry are in similar aqueous environments for both halocarbon interfaces. This is consistent with the picture derived from the previous experimental[71] and simulation studies[67] showing that water molecules contributing to this region are located in the region of the interface somewhat deeper into the water phase than those that come in direct contact with the organic phase, making them less likely to be affected by changes in the organic phase properties such as differences in polarity of CCl_4 versus chloroform.

The spectral fits also show that the frequency of the free OH peak for the chloroform–water interface is significantly lower than what has been found for other water–hydrophobic liquid systems including CCl_4–water, alkane–water, air–water, and solid hydrocarbon– and fluorocarbon–water interfaces.[27] For the chloroform–water interface, the center peak frequency for

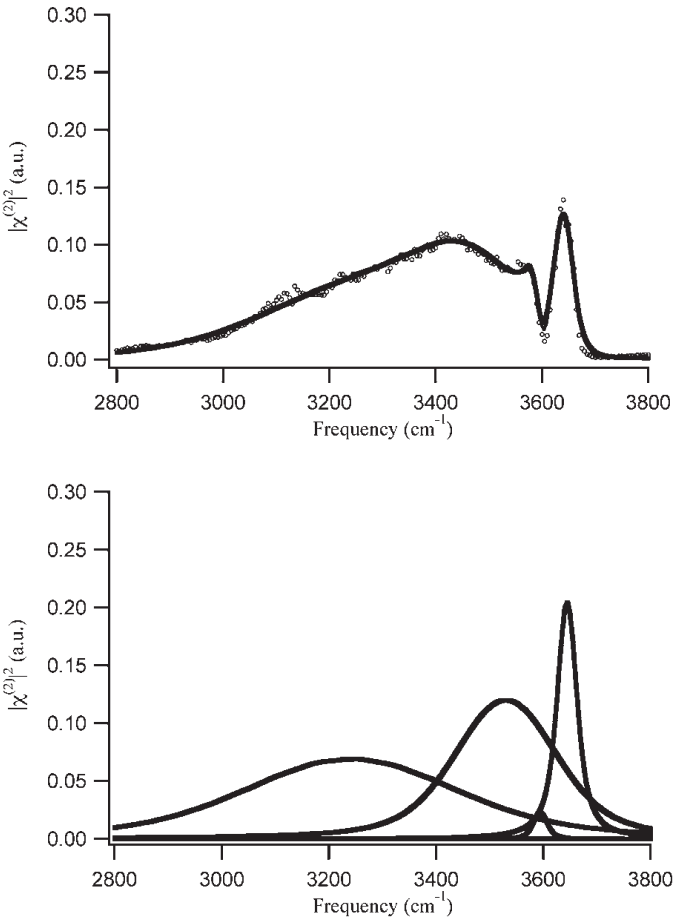

FIG. 4. The top plot shows the VSF spectrum of the chloroform–water interface where the circles are the data points and the solid line is the spectral fit. The bottom plot shows the composite peaks resulting from the spectral fit.

the free OH mode is found to be 3645 cm^{-1}, very close to the value of 3649 cm^{-1} for the uncoupled OH oscillator observed in bulk IR studies of HOD in $CDCl_3$.[72] The free OH frequency for chloroform–water is a shift of ~25 cm^{-1} relative to the free OH frequency of the CCl_4–water interface.[31] We attribute the red-shift to the interaction between the uncoupled OH modes of the straddling water molecules with their neighboring moderately polar chloroform molecules. Table I compares the free OH frequency determined for the chloroform–water interface to the values of the free OH frequencies seen previously for other liquid–liquid interfaces as well as the air–water interface. The relatively large red-shifted frequency for chloroform–water, relative to other free OH frequency values, indicates that there are substantial interactions taking place between the water and chloroform molecules relative to the other systems. The permanent dipole of chloroform molecules (1.04 D) that was not present in the other liquids previously studied (CCl_4 or *n*-alkanes) or in the vapor phase explains why a greater degree of interaction between the liquids occurs.

The free OH peak intensity is also lower for the chloroform–water interface VSF spectrum relative to that of CCl_4–water. We attribute this to a reduction in both the number of oriented water molecules and the degree of orientation of the molecules with a free OH that straddle the interface. The Gaussian width of the chloroform–water free OH was found to be broader than for the CCl_4–water interface. Both the decrease in peak

TABLE I. Comparison of free OH peak frequencies from previous VSFS studies to the current chloroform–water interface value.

Non-aqueous phase	Free OH frequency (cm^{-1})
Air	3706[46]
Alkanes	3674[26]
CCl_4	3669[31]
Chloroform	3645

intensity and increase in width are most likely a result of stronger water–chloroform interactions and also different types of water–chloroform complexes of different interaction strengths, geometries, and orientations. Similarly, formation of different interfacial complexes was found to be a factor in the relatively low free OH intensity in the alkane–water[26] study and lack of a distinct free OH feature in the DCE–water[32] study.

Another striking difference found in the isotopic dilution studies arises in region **2**, where both previous spectral fitting[31] and MD simulations[37] show that OH-bonded donor water molecules make a considerable contribution. At the highest D_2O concentration (Fig. 2), the donor OH mode appears at 3530 cm^{-1}, which is significantly blue-shifted from the values found for the analogous peak in isotopic dilution studies of the CCl_4–water (3440 cm^{-1})[31] and vapor–water (3420 cm^{-1})[46] interfaces. The large shift to higher frequency indicates that the hydrogen bonding environment of water at the inner-most region of the chloroform–water interface is significantly different than was observed for these other hydrophobic–water interfaces. It also indicates that water molecules contributing to the donor OH spectral region do not bond to neighboring water molecules to the degree that occurs for the CCl_4–water or vapor–water interfaces. We attribute the reduction in bonding character to a more mixed water–organic interfacial region in which neighboring water molecules in the inner-most region of the interface have a higher density of organic molecules around them and hence fewer opportunities for these donor OH modes to hydrogen bond to other water molecules. A schematic of the interfacial environment is shown in Fig. 5. It should be noted that the broadness of the mode, even at only 12% H_2O, contributes to a greater uncertainty in the assignment of the center peak frequency in comparison to the free OH. However, a good fit to the spectra cannot be achieved without a substantial shift to higher energies for the donor OH mode in comparison to the other non-polar liquid–liquid interfacial fitting results, indicating that the trend is real.

These experimental findings are in remarkable agreement with several MD studies over the past few years for these liquid–liquid interfacial systems. The studies by Walker et. al. involving calculations of the VSF spectra for the chloroform–water interface in *ssp* polarization reproduces the general features in the experimental spectrum.[64] The free OH frequency for the chloroform–water interface is calculated to be at lower energy relative to CCl_4, in good agreement with the results summarized in Table I. Further aspects of the MD study by Walker et al. that calculate the interfacial depth of the spectral response from different contributing water species show that the donor peak for the chloroform–water interface should appear at substantially higher energy compared to the calculated VSFS frequencies for the CCl_4–water interface, further corroborating the experimental results presented in the current study.[33] The MD results from Walker et al. also show the chloroform–water interface to be slightly wider than the

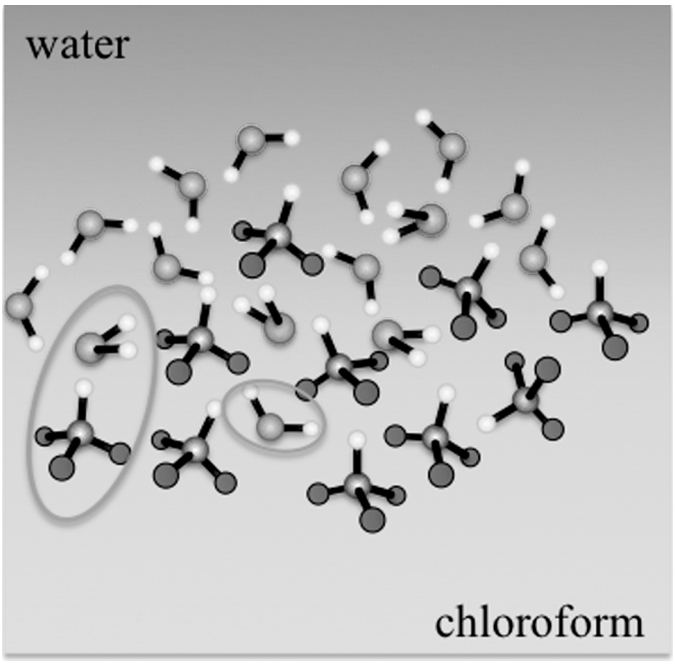

FIG. 5. Schematic depicting the chloroform–water interfacial region. The circles highlight water species present as a result of the interaction between the two liquids. (Left circle) Optimal chloroform–water interaction geometry and (right circle) very weakly hydrogen bound water molecules largely surrounded by chloroform molecules.

CCl_4–water interface.[33] In a study by Hore et al.[40] the orientation of interfacial water molecules is compared at different hydrophobic–water interfaces. The study concludes that the degree of interfacial water orientation is highly dependent on polarity of the hydrophobic phase. Moreover, the results predict that the degree of water structuring is greatest when the non-aqueous phase is the least polar, i.e., water molecules will have less net orientation at the chloroform–water interface than at the CCl_4–water interface. These results are again in excellent agreement with the observations here.

In a third MD study related to the work presented here, closer examination of the structure of the chloroform–water interface was done by calculating the order parameters for *both* the chloroform and the water molecules as a function of depth within the interface.[38] The results show that although a significant population of water molecules exist in the interfacial region that straddle the interface, there are also many water molecules that adopt an in-plane configuration. The in-plane oriented subset of water orientations is found at all liquid surfaces. For the unique chloroform–water interface this orientation serves to maximize the bonding-type interactions between the chloroform molecules that are oriented with the CH bond (which is the positive portion of the molecule's permanent dipole) pointed toward the aqueous phase and the water molecules. The resulting water–organic interactions are shown by the circle on the left of Fig. 5. Because CCl_4 molecules have no positive portion due to the zero permanent dipole moment, it is likely that there are not as many water molecules that adopt this in-plane configuration at the CCl_4–water interface. The MD result from the examination of the chloroform–water interface also helps explain the higher peak frequency of the donor OH peak for the chloroform–water interface when compared to that of CCl_4–water. With more water molecules adopting an in-plane configuration in order to interact with the chloroform molecules through the oxygen, the water–water interactions through the donor OH oscillator are weakened and the number of bonds is reduced, thereby increasing the peak frequency.

The last peak remaining in Fig. 4b to be discussed is the small peak found between the free and donor OH peaks fit at 3594 cm^{-1}. Its frequency and relatively narrow bandwidth indicate that water molecules responsible for this peak have weak bonding interactions with neighboring interfacial species. We attribute this mode to oriented water molecules in the interfacial region that are largely in contact with nearby chloroform molecules, thereby having minimal bonding interactions with other interfacial water molecules. Several bulk IR studies of dilute concentrations of water in chloroform show the symmetric OH vibrational stretch of water at ~3605 cm^{-1}, consistent with this assignment and further supporting the addition of this peak to fit the spectra.[73–76] Computational VSFS studies of the chloroform–water interface also show evidence of these types of weakly bonded water species in the spectral region above 3600 cm^{-1},[33] identified as water monomers and hydrogen bond acceptors present in the chloroform-rich portions of the interface. These very weakly bound water species are shown highlighted by the circle on the right of Fig. 5. Previous analysis of the CCl_4–water interface by VSFS and spectral fitting techniques[31] showed evidence of these types of water species. As shown in Fig. 1, the effect on the CCl_4–water spectrum is not as dramatic as is the case for the chloroform–water interfacial spectrum due, in part, to the interference of the peak at 3594 cm^{-1} with the spectral overlap of the free OH and donor OH modes present for the chloroform–water spectrum. Also, these types of very weakly interacting water molecules are likely found in greater numbers on the chloroform side of the interface due to increased miscibility of the two liquids, when compared to the CCl_4–water interactions, resulting in a larger spectral contribution. MD simulations indicate that these oriented water molecules penetrating into the organic phase up to 5 to 7 Å are indeed higher in number at the chloroform–water interface compared to CCl_4–water.[33]

CONCLUSION

Vibrational sum-frequency spectroscopy has been used here to study the structure of the chloroform–water interface. Mixtures of H_2O, HOD, and D_2O were used to deconvolute the different OH modes that contribute to the interfacial spectrum by fitting the spectra using tightly constrained values for the peak parameters. The picture that has emerged from the study presented here is that, for the chloroform–water interface, more mixing of the water and organic molecules occurs with stronger water–organic interactions and reduced water–water bonding interactions than is found for the CCl_4–water interface. Yet even with this increased interfacial mixing and weaker water–water interactions, the interfacial water still displays a significant degree of orientational ordering that is maintained even as weakly bound water molecules penetrate into the deeper and more organic-rich regions of the interface. Evidence for these conclusions comes from the wealth of information contained in the VSF spectral region around 3500 cm^{-1} including the frequency shifts in the modes corresponding to the free OH and its companion donor OH mode, and the

signature response from oriented interfacial water molecules surrounded by chloroform. Such information was not available from previous VSFS measurements of more polar organic–water interfaces, making these chloroform results particularly insightful and important.

These experimental spectroscopic studies of the chloroform–water interface provide a critical puzzle piece in the developing picture of molecular interactions that occur at the interface between water and organic liquids of varying polarity. Paramount in these studies is the confirmation of the importance of weak water–organic interfacial interactions at liquid–liquid interfaces and the variation of interfacial properties with relatively small changes in the molecular properties of the organic phase. The results demonstrate that there is a clear and understandable progression in the interfacial bonding and orientation of water with variation in the polarity and polarizability of the organic phase, confirmed by these chloroform–water studies. As the organic phase is varied from the non-polar alkanes,[26] to the more polarizable but still non-polar CCl_4,[31] and to the increasingly polar chloroform and DCE,[28,32] the strength and degree of bonding between interfacial organic–water molecules increases and interfacial water–water bonding interactions are reduced for those molecules closest to the dividing surface. Orientational ordering of interfacial water persists but is reduced relative to what is present at water next to a non-polar organic liquid such as CCl_4, but is still larger than that found for DCE. Simulations support these conclusions and attribute them to the water–organic interactions that help establish a field across the interface, which can facilitate ion adsorption.[7,40]

Accompanying the increased interaction and subsequent mixing of the water with the organic phase is an increase in the presence of oriented weakly bound water molecules that penetrate into the organic-rich portion of the interface. Such water species appeared in the earlier CCl_4–water interfacial studies but the spectral features of such water molecules were not nearly as dramatic as for the chloroform–water interface case.[31] In comparison to DCE, where such isotopic dilution experiments were not possible, spectral evidence from experiments[32] was ambiguous, although the simulations[37] indicated their presence. These VSFS chloroform–water interface results show a clear spectral signature from these weakly bound water species. Their prevalence and penetration into the more organic-rich interfacial regions is found to be intermediate between the CCl_4– and DCE–water interfacial studies.[33]

The evolving picture that is derived from VSFS studies of the bonding at liquid–liquid interfaces is clearly benefiting from the close coupling of these experiments with computational efforts in our laboratory and in others. The general molecular level interpretation gained by experimental measurements of the chloroform–water interface and those predicted by MD simulations are remarkably consistent, as they have been for the other liquid–liquid systems studied thus far,[29] reinforcing the value in combining such efforts for studying such complex interfaces. Further development of more accurate models for interfacial water will greatly benefit this effort.

The current understanding of these simple liquid–liquid interfaces is clearly in a relatively early stage with many more opportunities ahead for exploration. Such exploration is particularly important in light of the interesting new uses of this interface beyond the ongoing importance of its use in extraction and separation science. On-water reactions, assembly of nanoparticles, and green chemistry are examples of exciting new applications that take advantage of the unique environment of a liquid–liquid interface.[77–79] These chloroform–water studies make an important new contribution to our understanding of the molecular properties of water–organic interfaces and also to understanding the general characteristics of water at hydrophobic surfaces.

ACKNOWLEDGMENT

The authors would like to thank the National Science Foundation (Grant CHE-0652531) for funding this research.

1. M. Aguilar and J. L. Cortina, *Solvent Extraction and Liquid Membranes: Fundamentals and Applications in New Materials* (CRC Press, Boca Raton, FL, 2008).
2. R. G. Harrison, *Protein Purification Process Engineering* (Marcel Dekker, New York, 1994).
3. I. Benjamin, J. Chem. Phys. **97,** 1432 (1992).
4. I. Benjamin, J. Phys. Chem. B **109,** 13711 (2005).
5. D. Chandler, Nature (London) **437,** 640 (2005).
6. D. Chandler, Nature (London) **445,** 831 (2007).
7. T. M. Chang and L. X. Dang, J. Chem. Phys. **104,** 6772 (1996).
8. T. M. Chang and L. X. Dang, J. Phys. Chem. B **101,** 10518 (1997).
9. T. M. Chang and L. X. Dang, J. Chem. Phys. **108,** 818 (1998).
10. T. M. Chang, L. X. Dang, and K. A. Peterson, J. Phys. Chem. B **101,** 3413 (1997).
11. D. Michael and I. Benjamin, J. Chem. Phys. **114,** 2817 (2001).
12. L. R. Pratt and D. Chandler, J. Chem. Phys. **67,** 3683 (1977).
13. X. Chen, T. Yang, S. Kataoka, and P. S. Cremer, J. Am. Chem. Soc. **129,** 12272 (2007).
14. M. C. Gurau, S. M. Lim, E. T. Castellana, F. Albertorio, S. Kataoka, and P. S. Cremer, J. Am. Chem. Soc. **126,** 10522 (2004).
15. G. M. Luo, S. Malkova, S. V. Pingali, D. G. Schultz, B. H. Lin, M. Meron, I. Benjamin, P. Vanysek, and M. L. Schlossman, J. Phys. Chem. B **110,** 4527 (2006).
16. G. M. Luo, S. Malkova, S. V. Pingali, D. G. Schultz, B. H. Lin, M. Meron, T. J. Graber, J. Gebhardt, P. Vanysek, and M. L. Schlossman, Electrochem. Commun. **7,** 627 (2005).
17. D. M. Mitrinovic, A. M. Tikhonov, M. Li, Z. Q. Huang, and M. L. Schlossman, Phys. Rev. Lett. **85,** 582 (2000).
18. D. M. Mitrinovic, Z. J. Zhang, S. M. Williams, Z. Q. Huang, and M. L. Schlossman, J. Phys. Chem. B **103,** 1779 (1999).
19. M. L. Schlossman, Curr. Opin. Colloid Interface Sci. **7,** 235 (2002).
20. W. H. Steel and R. A. Walker, Nature (London) **424,** 296 (2003).
21. W. H. Steel and R. A. Walker, J. Am. Chem. Soc. **125,** 1132 (2003).
22. A. M. Tikhonov, D. M. Mitrinovic, M. Li, Z. Q. Huang, and M. L. Schlossman, J. Phys. Chem. B **104,** 6336 (2000).
23. M. Aoki, Y. Ohashi, and S. Masuda, Surf. Sci. **532,** 137 (2003).
24. N. S. Holmes and J. R. Sodeau, J. Phys. Chem. A **103,** 4673 (1999).
25. J. E. Schaff and J. T. Roberts, J. Phys. Chem. **100,** 14151 (1996).
26. M. G. Brown, D. S. Walker, E. A. Raymond, and G. L. Richmond, J. Phys. Chem. B **107,** 237 (2003).
27. C. L. McFearin, D. K. Beaman, F. G. Moore, and G. L. Richmond, J. Phys. Chem. C **113,** 1171 (2009).
28. C. L. McFearin and G. L. Richmond, J. Mol. Liq. **136,** 221 (2007).
29. F. G. Moore and G. L. Richmond, Acc. Chem. Res. **41,** 739 (2008).
30. L. F. Scatena, M. G. Brown, and G. L. Richmond, Science (Washington, D.C.) **292,** 908 (2001).
31. L. F. Scatena and G. L. Richmond, J. Phys. Chem. B **105,** 11240 (2001).
32. D. S. Walker, M. Brown, C. L. McFearin, and G. L. Richmond, J. Phys. Chem. B **108,** 2111 (2004).
33. D. S. Walker and G. L. Richmond, J. Phys. Chem. C **112,** 201 (2008).
34. A. Morita and J. T. Hynes, Chem. Phys. **258,** 371 (2000).
35. P. Jedlovszky, J. Phys.: Condens. Matter **16,** S5389 (2004).
36. P. Jedlovszky, A. Vincze, and G. Horvai, Phys. Chem. Chem. Phys. **6,** 1874 (2004).
37. D. S. Walker, F. G. Moore, and G. L. Richmond, J. Phys. Chem. C **111,** 6103 (2007).
38. D. K. Hore, D. S. Walker, L. MacKinnon, and G. L. Richmond, J. Phys. Chem. C **111,** 8832 (2007).

39. D. K. Hore, D. S. Walker, and G. L. Richmond, J. Am. Chem. Soc. **129,** 752 (2007).
40. D. K. Hore, D. S. Walker, and G. L. Richmond, J. Am. Chem. Soc. **130,** 1800 (2008).
41. N. Sieffert and G. Wipff, J. Phys. Chem. B **110,** 4125 (2006).
42. R. Diss and G. Wipff, Phys. Chem. Chem. Phys. **7,** 264 (2005).
43. B. Schnell, R. Schurhammer, and G. Wipff, J. Phys. Chem. B **108,** 2285 (2004).
44. P. Jost, A. Chaumont, and G. Wipff, Supramol. Chem. **15,** 133 (2003).
45. M. Baaden, F. Berny, C. Madic, R. Schurhammer, and G. Wipff, Solvent Extr. Ion Exch. **21,** 199 (2003).
46. E. A. Raymond, T. L. Tarbuck, M. G. Brown, and G. L. Richmond, J. Phys. Chem. B **107,** 546 (2003).
47. C. S. Tian and Y. R. Shen, Chem. Phys. Lett. **470,** 1 (2009).
48. R. W. Boyd, *Nonlinear Optics* (Academic Press, San Diego, CA, 2003), 2nd ed.
49. A. G. Lambert, P. B. Davies, and D. J. Neivandt, Appl. Spectrosc. Rev. **40,** 103 (2005).
50. P. B. Miranda and Y. R. Shen, J. Phys. Chem. B **103,** 3292 (1999).
51. A. J. Moad and G. J. Simpson, J. Phys. Chem. B **108,** 3548 (2004).
52. G. Richmond, Annu. Rev. Phys. Chem. **52,** 357 (2001).
53. H. F. Wang, W. Gan, R. Lu, Y. Rao, and B. H. Wu, Int. Rev. Phys. Chem. **24,** 191 (2005).
54. X. D. Zhu, H. Suhr, and Y. R. Shen, Phys. Rev. B **35,** 3047 (1987).
55. J. Lobau and K. Wolfrum, J. Opt. Soc. Am. B **14,** 2505 (1997).
56. X. Zhuang, P. B. Miranda, D. Kim, and Y. R. Shen, Phys. Rev. B **59,** 12632 (1999).
57. M. L. Lang and W. L. Wolfe, Appl. Opt. **22,** 1267 (1983).
58. M. A. Czarnecki, J. P. Hawranek, and W. Wrzeszcz, J. Mol. Struct. **275,** 111 (1992).
59. T. G. Goplen, D. G. Cameron, and R. N. Jones, Appl. Spectrosc. **34,** 657 (1980).
60. G. M. Hale and M. R. Querry, Appl. Opt. **12,** 555 (1973).
61. E. A. Raymond and G. L. Richmond, J. Phys. Chem. B **108,** 5051 (2004).
62. F. G. Moore, K. A. Becraft, and G. L. Richmond, Appl. Spectrosc. **56,** 1575 (2002).
63. C. D. Bain, P. B. Davies, T. H. Ong, R. N. Ward, and M. A. Brown, Langmuir **7,** 1563 (1991).
64. D. S. Walker and G. L. Richmond, J. Phys. Chem. C **111,** 8321 (2007).
65. B. Auer, R. Kumar, J. R. Schmidt, and J. L. Skinner, Proc. Natl. Acad. Sci. USA **104,** 14215 (2007).
66. D. S. Walker, D. K. Hore, and G. L. Richmond, J. Phys. Chem. B **110,** 20451 (2006).
67. D. S. Walker and G. L. Richmond, J. Am. Chem. Soc. **129,** 9446 (2007).
68. B. M. Auer and J. L. Skinner, J. Chem. Phys. **129,** 214705 (2008).
69. V. Buch, T. L. Tarbuck, G. L. Richmond, H. Groenzin, I. Li, and M. J. Schultz, J. Chem. Phys. **127,** 204710 (2007).
70. N. Ji, V. Ostroverkhov, C. S. Tian, and Y. R. Shen, Phys. Rev. Lett. **1,** 096102 (2008).
71. D. E. Gragson and G. L. Richmond, J. Phys. Chem. B **102,** 3847 (1998).
72. J. R. Downey and G. R. Choppin, Spectrochim. Acta, Part A **30,** 37 (1974).
73. G. R. Choppin and J. R. Downey, Jr., Spectrochim. Acta, Part A **30,** 43 (1974).
74. J. C. Dobrowolski and M. H. Jamroz, J. Mol. Struct. **293,** 147 (1993).
75. H. Graener and G. Seifert, J. Chem. Phys. **98,** 36 (1993).
76. H. Graener, G. Seifert, and A. Laubereau, Chem. Phys. **175,** 193 (1993).
77. Y. S. Jung and R. A. Marcus, J. Am. Chem. Soc. **129,** 5492 (2007).
78. S. Narayan, J. Muldoon, M. G. Finn, V. V. Fokin, H. C. Kolb, and K. B. Sharpless, Angew. Chem., Int. Ed. **44,** 3275 (2005).
79. C. N. R. Rao and K. P. Kalyanikutty, Acc. Chem. Res. **41,** 489 (2008).